

Scalable fabric tactile sensor arrays for soft bodies

Nathan Day¹, Jimmy Penaloza², Veronica J Santos²  and Marc D Killpack^{1,3} 

¹ Mechanical Engineering Dept., Brigham Young University, Provo, UT, United States of America

² Mechanical and Aerospace Engineering Dept., University of California, Los Angeles, CA, United States of America

E-mail: marc_killpack@byu.edu

Received 2 October 2017, revised 14 February 2018

Accepted for publication 26 February 2018


Published 4 April 2018



Abstract

Soft robots have the potential to transform the way robots interact with their environment. This is due to their low inertia and inherent ability to more safely interact with the world without damaging themselves or the people around them. However, existing sensing for soft robots has at least partially limited their ability to control interactions with their environment. Tactile sensors could enable soft robots to sense interaction, but most tactile sensors are made from rigid substrates and are not well suited to applications for soft robots which can deform. In addition, the benefit of being able to cheaply manufacture soft robots may be lost if the tactile sensors that cover them are expensive and their resolution does not scale well for manufacturability. This paper discusses the development of a method to make affordable, high-resolution, tactile sensor arrays (manufactured in rows and columns) that can be used for sensorizing soft robots and other soft bodies. However, the construction results in a sensor array that exhibits significant amounts of cross-talk when two taxels in the same row are compressed. Using the same fabric-based tactile sensor array construction design, two different methods for cross-talk compensation are presented. The first uses a mathematical model to calculate a change in resistance of each taxel directly. The second method introduces additional simple circuit components that enable us to isolate each taxel electrically and relate voltage to force directly. Fabric sensor arrays are demonstrated for two different soft-bodied applications: an inflatable single link robot and a human wrist.

Keywords: cross-talk, soft robot, flexible tactile sensor array, scalable, soft body sensing

 Supplementary material for this article is available [online](#)

(Some figures may appear in colour only in the online journal)

1. Introduction

1.1. Soft robots

Research into fabricating and controlling soft robots has recently increased significantly [1–9]. This is in part because the demand for robots that can safely interact physically with their surroundings is increasing dramatically. Rigid robots are expensive and are typically programmed to avoid unwanted contact with their surroundings. Soft robots have the potential to be much cheaper and can make extensive contact with their

surroundings without causing damage to themselves or their environment. Additionally, physical interaction with a traditional robot often requires high bandwidth control and sensing in order to be safe. Instead, many soft robots are passively compliant and therefore inherently safer when interacting with their environment. Although soft robots may be able to more safely make contact with their environment, without contact sensing the benefit of this capability is very limited. Soft, cheap, scalable, high-resolution sensing is a key to exploiting this capability for soft robots. Whole body skins for robots require a scalable solution for large areas over curved surfaces, with the additional design criterion of flexibility for soft robots.

³ Author to whom any correspondence should be addressed.

1.2. Tactile sensing

Tactile sensing has been developed for decades because of its promise to improve a robot's ability to interact with the world using closed-loop feedback control. One of the most popular methods of tactile sensing uses material that changes resistance when compressed in series with a constant value resistor. This results in a voltage divider circuit that allows a changing voltage to be read from the node between the two resistive elements. This method is demonstrated in multiple papers [10–15].

Our goal in the design and manufacturing of our sensor was to make it scalable as well as soft and deformable for integration with a soft robot or other soft body such as a human arm. The sensor presented in this paper is made of conductive, non-conductive, and resistive fabric materials. The voltage output of each taxel (or individual tactile sensor unit) is directly correlated with how much the resistive fabric is compressed.

To decrease the amount of electronics required while increasing sensing resolution, we built a sensor that operates in a grid with rows and columns (see figure 1). A single column is powered with 5V, while simultaneously reading the voltage along a single row using an analog to digital converter (ADC). Where the column and the row intersect, a taxel is formed, and a voltage reading can be obtained and correlated to force. This method increases the sensing resolution while decreasing the amount of electronics that would be required for individual sensors. However, this form of sensor array may exhibit cross-talk when multiple taxels are activated simultaneously. Addressing this problem is one contribution of our work. Two methods are introduced: the use of a mathematical model to calculate changes in resistance, and the minimal use of additional simple circuit components to electrically isolate taxels.

2. Related work

Related to our work in this paper, other researchers have begun to examine different tactile sensing methods for soft bodies. Rogers *et al* [16] discuss different types of materials that are used in stretchable electronics, and mainly focus on organic-based devices such as those discussed in [17]. A discussion of fabric-based tactile sensors was not included. Other examples of flexible sensors are shown in Someya *et al* [18] and [19] demonstrating a conformable, flexible network of pressure sensors using organic transistors. The manufacturing of such sensors typically requires a clean room and sophisticated prototyping processes and equipment along with domain-specific expertise. The use of transistors also adds complexity to the circuit. Cross-talk was mentioned in [18], but a solution for cross-talk compensation was never proposed. Further examples of tactile sensors include Yamaguchi *et al* [20], who have shown that they could use optical sensing of a transparent soft material on a gripper to improve performance while gripping tools. Sareh *et al* [21] have used tactile sensing on a soft robot prototype for minimally invasive surgeries. Although both of

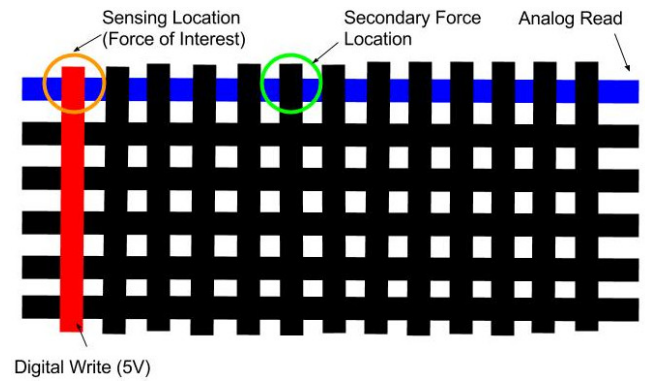


Figure 1. Representative scenario for parallel parasitic cross-talk.

these tactile sensor designs were created specifically for soft robots, it is unclear if they would generalize and scale well for large surface areas and soft bodies, as we show in this paper.

Specifically related to our variable resistance tactile sensing method, many researchers have explored methods of tactile sensing using voltage drive lines and analog to digital conversion lines set in a grid to decrease the number of electronics and increase resolution. The difficulty with this architecture is that the taxels are no longer isolated circuits and cross-talk occurs. Two types of cross-talk are possible: mechanical cross-talk and parallel parasitic cross-talk. Mechanical cross-talk is caused by indirectly straining material when pressing on an adjacent taxel. This effect was discussed in Canavese *et al* [11]. However, Canavese *et al* never tested for parallel parasitic cross-talk. Parallel parasitic cross-talk is caused by resistors in parallel that influence the voltage output when two or more non-adjacent nodes are compressed simultaneously. An example of when this type of cross-talk would occur is shown in figure 1.

Past methods for cross-talk compensation, although effective at eliminating current leakage (see [22, 23]), do not eliminate parallel parasitic cross-talk. Other research that has attempted to address this problem requires complicated circuitry which increases cost and complexity for manufacturing (see [14, 24, 25]).

Our initial tactile sensors were based on work performed by researchers at the Georgia Institute of Technology [10]. Fabric taxels were individually sewn and wired, which limits the scalability of the design due to its labor intensive nature and increased cost and circuit complexity. Another problem with this design is that when isolating each taxel electrically, the sensing resolution is very limited. This is due to the size of each taxel and due to the electronics required for a large array of sensors. The taxels can be made smaller, but then the number and complexity of electronics needed to get information from each taxel greatly increases. For example, in [10] since each taxel requires a single ADC—100 taxels would require 100 ADCs. However, our methods allow us to design and build a sensor that, in addition to being flexible, low-cost, and easily made in-house, also scales well to large areas and does not require complex circuitry.

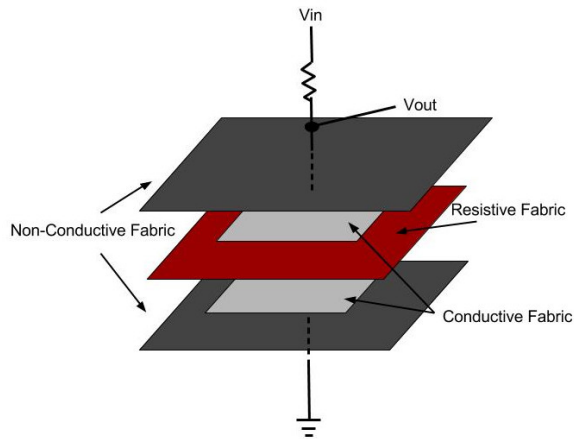


Figure 2. Construction of an individual taxel.



Figure 3. Sensor construction with columns and rows of conductive fabric. The gray resistive material is folded back to reveal columns of conductive material. Metal snaps are located at the top of each column.

3. Sensor design and construction

Individual taxels were typically constructed following the design shown in figure 2, similar to those described in [10]. We employed the same materials used in [10] in the new grid-style sensor.

We used an iron-on adhesive to glue the conductive fabric to the non-conductive spandex material. Strips of conductive fabric were glued to one side of the spandex material in rows, while columns of the conductive fabric were glued to a spandex fabric opposite. A large piece of resistive material (EeonTex LG-SLPA-20K supplied by Eeonyx) was then placed between the two layers of spandex with the columns and rows of conductive material facing the resistive material (see figure 3).

Metal snaps were connected to the ends of the conductive fabric strips so that wires could be soldered to them. We used an Arduino Mega's ADC channels to record from the rows and we used the digital outputs to power the columns of the sensor. To obtain information from each taxel using the Arduino, we read from every ADC channel while cycling through each 5V digital I/O pin. Using 27 I/O pins and 11 ADCs we were able to read from 297 taxel positions at a rate of approximately 80 Hz with un-optimized code on the Arduino Mega.

There are some limitations for our current hardware design. The minimum spatial resolution is limited by the conductive filament used. For the first application we show on a

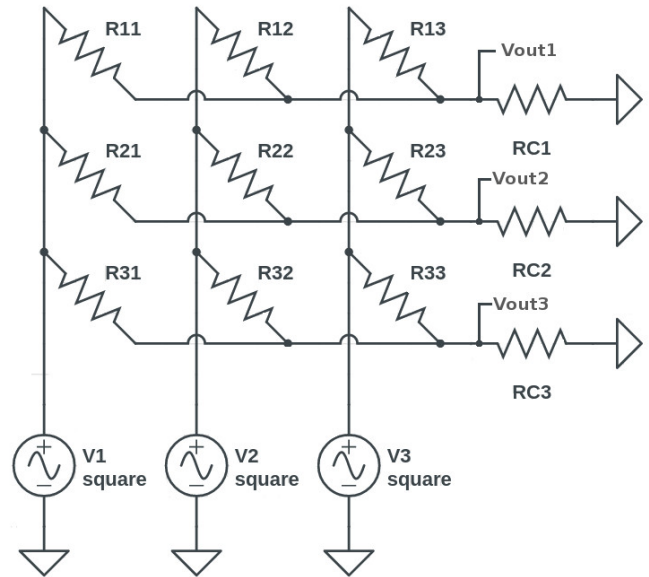


Figure 4. 3×3 simplified high resolution sensor.

soft robot, we used 3/8" strips of conductive fabric, but there is conductive thread that is available and should also work in a similar manner. Additionally, since we currently use metal snaps, our row and column sizes are limited by the size of the snaps. However, that is not a fundamental limitation and could be resolved if finer spatial resolution is needed. Finally, in terms of sampling real-world phenomenon at high frequencies, we fully expect the mechanical response of the fabric to be much slower than the electrical response. Therefore the limit to sampling any kind of impulsive force would likely be the actual fabric mechanics or the sampling rate of the ADC.

4. Cross-talk compensation

Two methods of cross-talk compensation on this high resolution sensor will be discussed in the following sections. The first method requires fewer electrical components along with a mathematical model we developed for estimating cross-talk. Using the cross-talk model, we can determine a change in resistance for each taxel, which can be directly correlated to force. The second method is similar to methods in [24], where the resistor of interest is isolated through the use of multiplexers. However, instead of using multiplexers to create open circuits, diodes are used to restrict the flow of current and simplify the control circuitry. The benefits of each method will be discussed in the following sections.

4.1. Cross-talk compensation by modeling of the circuit

4.1.1. Mathematical model. Initial tests of a grid tactile sensor prototype showed that there was a significant amount of parallel parasitic cross-talk when compressing several taxels in the same row. In order to compensate for this cross-talk, we developed a model of the circuit that would estimate the behavior of the cross-talk. Figure 4 shows a simplified circuit schematic of a 3 row by 3 column grid sensor. R_{kj} for $k = 1, 2, 3$ and $j = 1, 2, 3$ represents the changing resistance

of each node when the resistive fabric is compressed. R_{C_1} through R_{C_3} represent the constant value resistors needed to form a voltage divider. V_1 , V_2 , and V_3 represent the alternating square waves used to power each column individually and V_{out1} , V_{out2} , V_{out3} represent the location where the voltages are read by the ADCs.

Using Kirchoff's current and voltage laws and this simplified 3×3 version of the high resolution tactile sensor, our model showed that the voltage output, V_{out} , is a function of all the resistance values corresponding to the same row. For example, V_{out1} only depends on the resistance values of the first row. Equation (1) shows the form of this relationship.

$$V_{out1} = \frac{aV_3 + bV_2 + cV_1}{R_{11}R_{12}R_{13} + a + b + c} \quad (1)$$

Where:

$$a = R_{11}R_{12}R_{C_1}$$

$$b = R_{11}R_{13}R_{C_1}$$

$$c = R_{12}R_{13}R_{C_1}$$

Since each voltage input is activated one at a time using alternating square waves, the equation simplifies depending on which channel is powered. If $V_1 = 5V$, then $V_2 = V_3 = 0$, equation (1) then simplifies to:

$$V_{out1,1} = \frac{cV_1}{R_{11}R_{12}R_{13} + a + b + c}. \quad (2)$$

Where $V_{out1,1}$ would represent the voltage reading at node R_{11} when only V_1 is powered. This shows that the voltage reading of one row is not only dependent on the change of resistance between where the column and row intersect, but on each change of resistance that occurs along the entire row. This is what makes it impossible to directly correlate force to V_{out} .

4.1.2. Cross-talk simulation. To check the validity of equation (2) and our ability to estimate cross-talk, we built a simple simulation in MATLAB to see if the cross-talk model behaved like the cross-talk in the physical sensor. The experiment consisted of holding two resistor values on a single row constant in simulation while increasing pressure on the third variable resistor on the same row. Without changing the force on the two resistors, the voltage readings dropped as force on the third resistor increased. This demonstrated the effect of parallel parasitic cross-talk. We then compared the results from our simulation to data collected from a small-scale tactile sensor (3 rows by 3 columns) using the same method. This time, we applied a constant force or pressure to the first two taxels to get a constant resistance while simultaneously increasing pressure on the third resistor in the same row. Figure 5 shows that the simulated and actual responses were comparable. Any apparent differences were such that we expected to be able to compensate for them through calibration.

Based on the results of the above comparison, we saw that the voltage outputs were a function of all resistors corresponding to the same row. Since the actual resistance at each

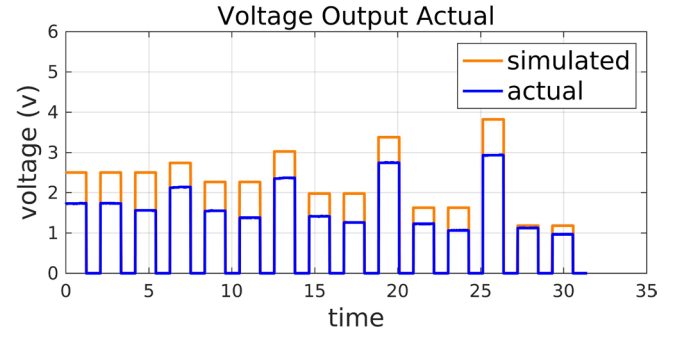


Figure 5. A comparison of simulated and actual tactile sensor cross-talk.

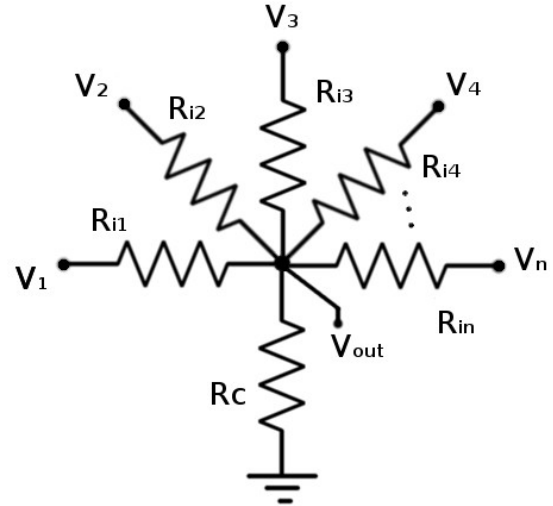


Figure 6. A simplified circuit showing a single row as a branching circuit.

node is independent of all other resistances, we wanted a method to solve for the resistance directly based on the voltage readings obtained from each row.

From equation (2) we can see that V_{out} is only a function of the row resistances and a known input voltage which allows us to analyze the circuit of a single row at a time. Figure 6 shows what a single row circuit would look like with R_{kj} representing the j number of resistances of the k th row, R_{C_k} representing the constant resistor in the voltage divider, V_j representing the cycling square waves, and $V_{out,kj}$ representing the voltage output on the k th row when the j th column is powered.

Our known variables are V_k and $V_{out,kj}$ at time t (where t is a discrete time step), and R_{C_k} which is fixed. The goal is to find the R_{kj} 's. Given the voltage drop across a resistor ΔV , we know that $\Delta V = iR$, and that the sum of the currents into a node is equal to the sum of the currents leaving. Therefore, we can show that the current through the constant resistor, i_{C_k} , is

$$i_{C_k} = \frac{V_1 - V_{out,k}}{R_{11}} + \frac{V_2 - V_{out,k}}{R_{12}} \dots + \frac{V_n - V_{out,k}}{R_{1n}}. \quad (3)$$

At time $t = 1$, V_1 is on and the rest of the input voltages are 0, and we sample $V_{out,k1}$. At time $t = 2$, V_2 is on and the rest of the input voltages are off, and we sample $V_{out,k2}$, etc. A matrix, $V_{\Delta,k}$, can be constructed for time $t = 1 \dots n$ where n is the total number of columns. We can then create an $n \times n$

matrix of ΔV 's for calculating the resistances of a single row as follows:

$$\mathcal{V}_{\Delta,k} = \begin{bmatrix} (V_1 - V_{out,k1}) & -V_{out,k1} & -V_{out,k1} & \dots & -V_{out,k1} \\ -V_{out,k2} & (V_2 - V_{out,k2}) & -V_{out,k2} & \dots & -V_{out,k2} \\ -V_{out,k3} & -V_{out,k3} & (V_3 - V_{out,k3}) & \dots & -V_{out,k3} \\ \vdots & \vdots & \vdots & \ddots & \vdots \\ -V_{out,kn} & -V_{out,kn} & -V_{out,kn} & \dots & (V_n - V_{out,kn}) \end{bmatrix} \quad (4)$$

Using what we know from equation (3), we get current if we divide ΔV by R . We define \mathcal{R}_k as the array of inverse resistances.

$$\mathcal{R}_k = \left[\frac{1}{R_{k1}} \quad \frac{1}{R_{k2}} \quad \frac{1}{R_{k3}} \quad \dots \quad \frac{1}{R_{kn}} \right]^T \quad (5)$$

The current i_{C_k} at any time $t = 1 \dots n$ is known and can be shown to be

$$\mathcal{I}_{C_k} = \left[\frac{V_{out,k1}}{R_{C_k}} \quad \frac{V_{out,k2}}{R_{C_k}} \quad \frac{V_{out,k3}}{R_{C_k}} \quad \dots \quad \frac{V_{out,kn}}{R_{C_k}} \right]^T. \quad (6)$$

Given these matrices, we can show that the following is true:

$$\mathcal{I}_{C_k} = \mathcal{V}_{\Delta,k} \mathcal{R}_k. \quad (7)$$

Remembering that the unknowns we wish to find in this equation are the inverse of the elements in \mathcal{R}_k , they can be solved for in the following manner:

$$\mathcal{R}_k = (\mathcal{V}_{\Delta,k})^{-1} \mathcal{I}_{C_k}. \quad (8)$$

This solution only represents the inverse of the resistance values for a single row, k . All the resistances can be solved for simultaneously if we apply this method to each row. A block matrix can be formed using this solution for the k th row. Using this matrix we can find the resistance values for every node. The form of this solution is shown in equation (9) where m represents the total number of rows.

$$\begin{bmatrix} \mathcal{I}_{C1} \\ \mathcal{I}_{C2} \\ \mathcal{I}_{C3} \\ \vdots \\ \mathcal{I}_{Cm} \end{bmatrix} = \begin{bmatrix} \mathcal{V}_{\Delta,1} & \emptyset & \emptyset & \emptyset & \emptyset \\ \emptyset & \mathcal{V}_{\Delta,2} & \emptyset & \emptyset & \emptyset \\ \emptyset & \emptyset & \mathcal{V}_{\Delta,3} & \emptyset & \emptyset \\ \emptyset & \emptyset & \emptyset & \ddots & \emptyset \\ \emptyset & \emptyset & \emptyset & \emptyset & \mathcal{V}_{\Delta,m} \end{bmatrix} \begin{bmatrix} \mathcal{R}_1 \\ \mathcal{R}_2 \\ \mathcal{R}_3 \\ \vdots \\ \mathcal{R}_m \end{bmatrix} \quad (9)$$

4.1.3. Sensor calibration. To illustrate the performance of the sensor after applying the result from equation (9) to the raw data, supplemental video 1 (stacks.iop.org/JMM/28/064004/mmedia) shows us compressing multiple taxels in the same and different rows on a flat surface.

The next step was to relate the measured values to force. Instead of using voltage in the cross-talk compensation code, we used the actual ADC readings reported from the Arduino Mega while assuming that the conversion between voltage and ADC values could be included in our calibration. For example, instead of using 5V for V_k we substituted in the 10 bit ADC representation of 5V, and instead of $V_{out,kj}$ being reported as values between 0V and 5V, they were reported as values between 0 and 1024. One further note is that the sensor

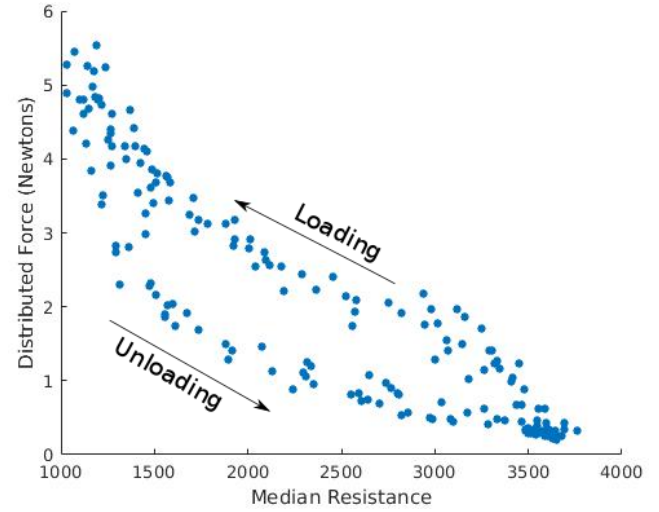


Figure 7. A plot showing the behavior of hysteresis in the material.

performs better when a low value resistor is used for the constant value resistor R_{C_k} since a lower resistor value increases the voltage range of each taxel. 330Ω resistors worked well for our specific setup in the first demonstration application on a soft robot.

The tactile sensor was calibrated on a flat, rigid surface by pressing a force torque sensor with an attached square plate against multiple taxels. We then summed the total number of active taxels and divided the force by that number to get a force per taxel (or distributed force) value. We then took the calculated resistance of the active taxels, found the median, and correlated it with the force per taxel value. Figures 7–9 show the characteristic behavior of the sensor in four different scenarios: (1) the sensor is quickly loaded and unloaded multiple times to demonstrate the mechanical hysteresis of the fabric, (2) a load is applied at a slower rate of $1 \frac{N}{s}$, (3) a load is applied at a faster rate of $5 \frac{N}{s}$, and (4) the sensor is loaded to a specific value and unloaded to non-zero values multiple times (where the time dependence is represented by the colors transitioning from dark blue to yellow). Our main focus was to perform a simple calibration of the sensor and use it on a single link robot arm for validation, so we did not attempt to compensate for hysteresis in this work. Methods can be employed such as those discussed in [26] to overcome the effects of hysteresis. Ignoring the effects of hysteresis, we used the linear calibration from figure 8 for the loading curve and applied it to the sensor for testing. Figure 8 shows that calibration was fairly consistent for different rates of loading as well.

Once the calibration was applied to the tactile sensor, we tested its accuracy and repeatability with the sensor array placed on a flat rigid surface. A 1.5 inch square of acrylic was pressed against the sensor while measuring the force with a force-torque sensor. The estimated force from each individual taxel was summed together to estimate a *total* applied force. Figure 10 shows the total estimated force compared to the actual applied force reported by the force-torque sensor. Although there is error and hysteresis, the accuracy for such large total forces is very encouraging.

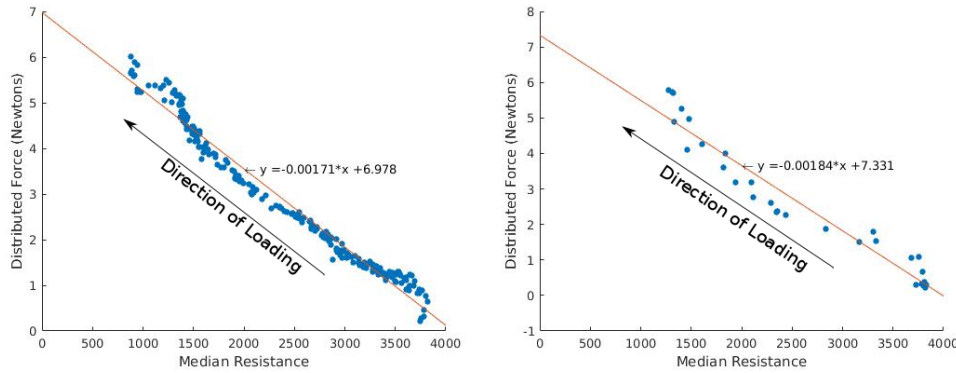


Figure 8. Left: a plot of the median of a group of taxel resistance values versus force per taxel with a loading rate of $1 \frac{N}{s}$. Right: a plot of the median of a group of taxel resistance values versus force per taxel with a loading rate of $5 \frac{N}{s}$.

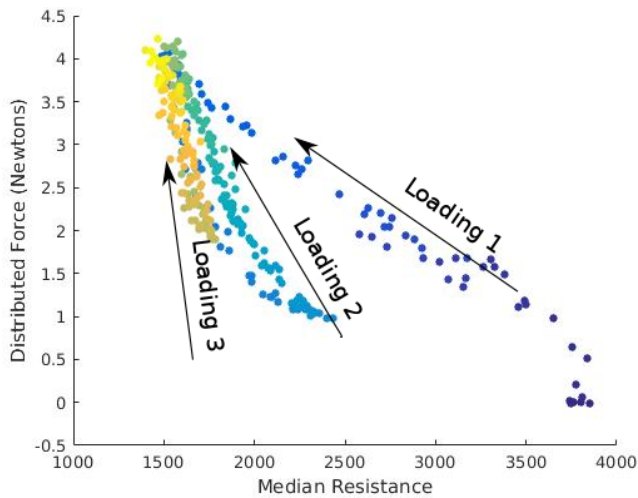


Figure 9. A plot showing repeated loading and unloading, where the sensor was unloaded to non-zero values before being loaded again.

4.1.4. Soft robot integration. Next, we wrapped the tactile sensor around the end of a single link inflatable robot. Figure 11 shows the sensor on the soft robot with a force torque sensor mounted on a stand. The robot was actuated so that it would press against the force-torque sensor. We pressed the robot link against the force-torque sensor multiple times while recording from both the tactile sensor array and the force-torque sensor. In order to compare the measurements from the tactile sensor array and the force-torque sensor, we summed the measured forces from each individual taxel to get a resultant force. Figure 12 shows how the tactile sensor array compared to the force-torque sensor. As was expected, the tactile sensor array measurements were noisier with the sensor wrapped around the soft robot limb than when it was tested on a flat, rigid surface. However, the overall accuracy and trends are quite good. Figure 12 shows the percent error of our estimated total force over time for the tactile sensor wrapped around the inflatable robot's limb. The large spikes represent the error due to the unmodeled effects of hysteresis occurring when the sensor is being unloaded. Any force estimates that were recorded as less than zero were assumed to be zero since the tactile sensor cannot be used to measure adhesive or negative forces. A video showing the collection

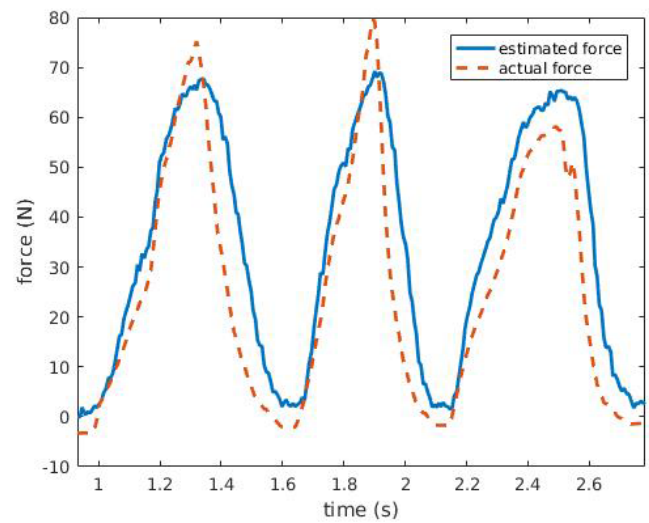


Figure 10. Sensor force estimate versus actual force when sensor is placed on a flat surface.

of the data reported in figure 11 is included as supplemental video 2.

Our sensor was developed as part of an SBIR Phase II program with NASA where we are currently working in collaboration with the startup company Pneubotics who has produced fabric-based, pneumatically-actuated soft robots, like the single joint shown in figure 11. In general, on our current soft robot hardware, we find that the main links of the robot do not bend or buckle and therefore tactile sensors on those sections would work well. However, sensors at the joints would obviously be deformed when the joint actuates and, similar to results in [10], would cause false positives if not compensated properly. However, because joint sensing for soft robots is still an open challenge as well, one possible application of our high resolution sensor is to integrate the sensors with the joints and use the data to learn models for joint deformation or configuration for soft robots.

4.2. Cross-talk compensation with additional circuitry

4.2.1. Electrical closure of parasitic current pathways. An alternative to the mathematical model compensation approach was developed to remove the source of cross-talk

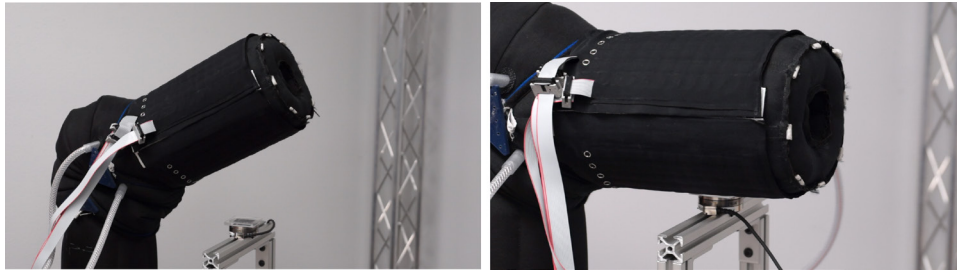


Figure 11. Images of tactile sleeve integrated onto a single link robot arm and the tactile sleeve being pressed against the force-torque sensor.

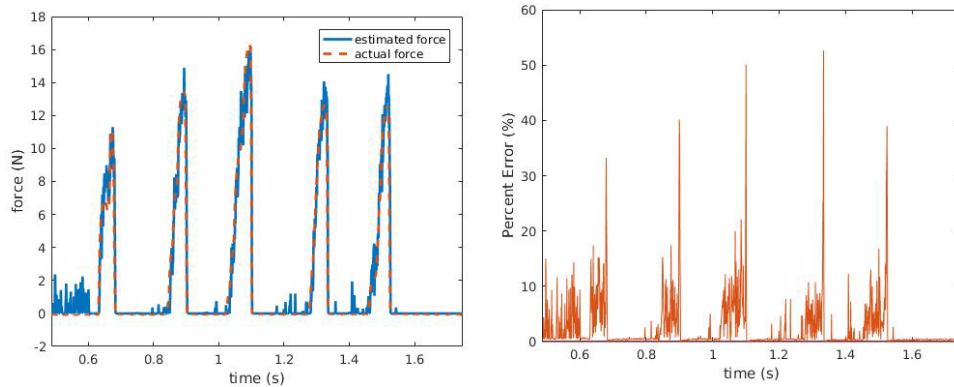


Figure 12. Left: the estimated force versus the actual force while the sensor is wrapped around an inflatable robot link. Right: this graph shows the percent error of the estimated force of the sensor on a single link robot.

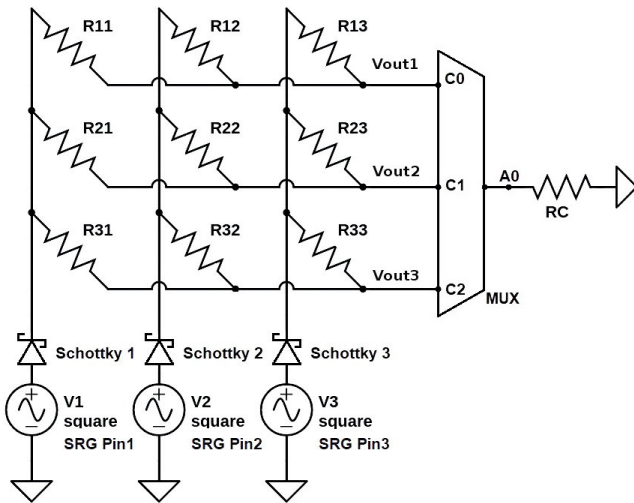


Figure 13. Alternative circuit diagram.

and is shown in figure 13. The alternative approach prevents cross-talk by electrically closing parasitic current pathways. The components used were a multiplexer, a shift register, and one Schottky diode for each column in the sensor array. The multiplexer (Texas Instruments CD74HC4067) has a break-before-make switching mechanism that prevents cross-talk by breaking the connections to all readouts except one before reading [27]. All the sensor readout rows have an open circuit except for the row being read, such that no parasitic current can flow in the open circuit directions. The constant value resistor R_C creates a voltage divider for the ADC to read from.

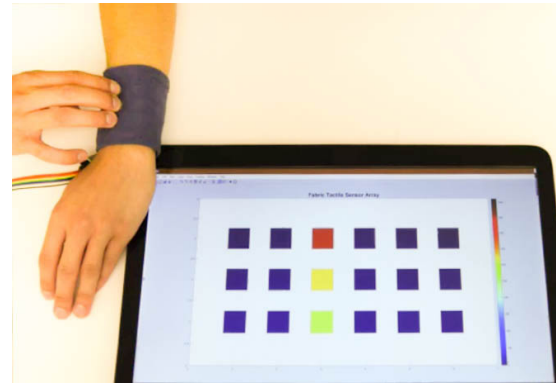


Figure 14. Wrist-worn fabric tactile sensor array.

The shift register (Texas Instruments 74HC595) is used to simultaneously update the voltage values of the columns. Using a shift register means that the digital outputs to the columns of the sensor are synchronized. Updating the outputs simultaneously allows us to avoid reading from the sensor before the current is steady. As shown in figure 13, the diodes are placed between the output of the shift register and the columns of the sensor. The diodes are used to prevent current back-flow into the shift register. As explained in the mathematical model, each sensor is modeled by a branching circuit or parasitic pathway; the cross-talk removal circuitry uses diodes to close off those branches and allows the output voltage of a sensor to be independent of the rest of the sensors in a given row. It should also be noted that the diodes used are Schottky diodes because they have a negligible voltage drop, thereby reducing loss in sensor resolution. The Schottky

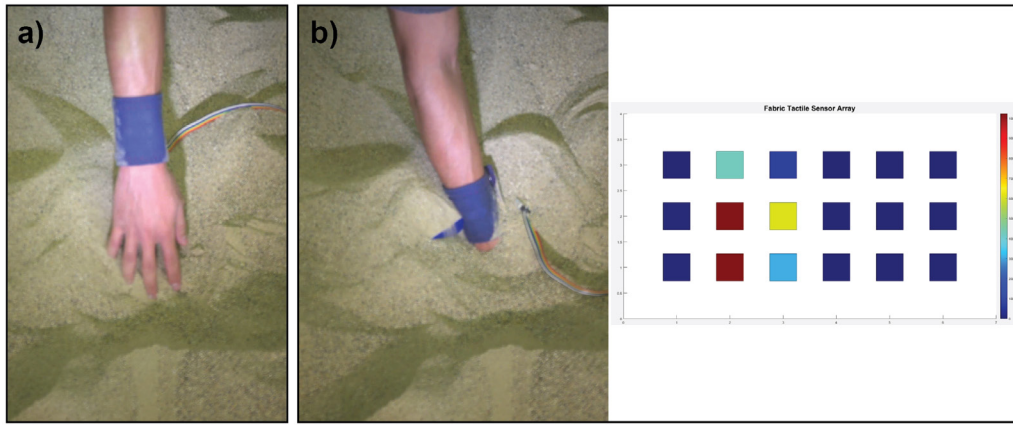


Figure 15. Wrist-worn fabric tactile sensor array (a) about to be immersed in sand and (b) measuring regions of contact and interaction forces between the wrist and a buried object.

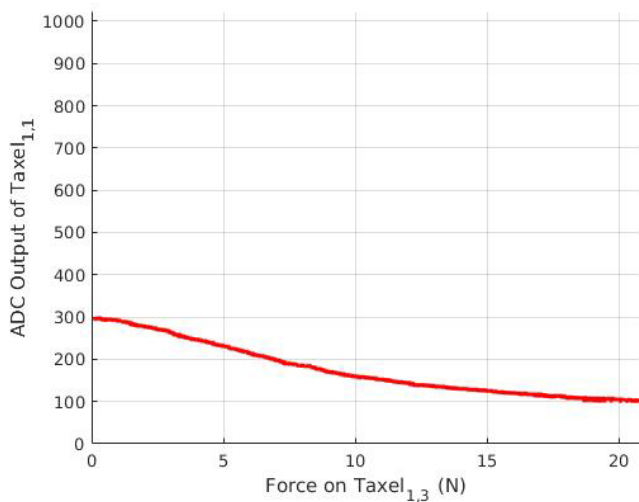


Figure 16. The effects of cross-talk without compensation.

diodes used are 20V, 1A and have a voltage drop of approximately 0.01–0.02 V. As shown in supplemental video 3, this circuit results in negligible parallel parasitic cross-talk.

4.2.2. Application on a human wrist. This second method of cross-talk compensation was demonstrated with a fabric tactile sensor array designed for a different soft body: the human body. Figures 14 and 15 show a 3×6 sensor array that has been wrapped around a human wrist for initial testing and in the intended application scenario. In this design, a ribbon cable with 28 AWG wire was used for electrical connections to columns instead of metal snaps. Individual wires were soldered with a flat tab and sandwiched between each adhesive strip of conductive tape and the underlying non-conductive fabric. Supplemental video 4 shows the wrist-worn fabric tactile sensor array being immersed in sand. The sensor array is able to measure regions of contact and approximate interaction forces between the wrist and a buried object.

4.3. Cross-talk compensation validation

In this paper, we presented two methods for cross-talk compensation. In this section, we present a final test to validate

the effectiveness of the two compensation methods in terms of removing the effects of cross-talk. In order to show how cross-talk affects the circuit, we took a simple 3×3 tactile sensor array and applied a constant load to taxel_{1,1} (which is the taxel in the first row and first column). An increasing force was then applied to taxel_{1,3} (first row, third column). The goal of this test was to see how sensor output (either voltage or estimated resistance depending on the method used) of taxel_{1,1} was affected by an applied load on taxel_{1,3}. In an ideal tactile sensor with no cross-talk, the reading for taxel_{1,1} would be independent of the load on taxel_{1,3} and would remain constant in this test. For a baseline comparison, figure 16 shows the results when no cross-talk compensation is applied. The figure clearly shows that cross-talk occurs, even in this simple 3×3 sensor array.

The same test was then performed for the two cross-talk compensation methods in order to validate their effectiveness. Figure 17 shows the effect of applying a constant load to taxel_{1,1} while increasing the force on taxel_{1,3} for each of the two cross-talk compensation methods.

As can be seen in figure 17, the two methods of cross-talk compensation virtually eliminate the effects of parallel parasitic cross-talk that can be seen in figure 16. Since the type of measurable unit differs for each compensation method, the Y-axis for each plot ranges from 0 to the full-scale range (FSR) of each method. The full-scale ranges for the resistance model and the extra circuitry method are 0–4000 and 0–1024, respectively. These values would then need to be calibrated to force for actual applications. In order to compare the effectiveness of the two methods, we also calculate the slopes of the plotted lines in figure 17. These slopes show the sensitivity of each compensation method to cross-talk during the loading. The slopes of the lines for both compensation methods stay relatively constant and near zero (especially compared to the slope of the uncompensated plot in figure 16). Table 1 shows the percent change of each line, which was calculated by taking the slope of each line and dividing it by the FSR.

Although both compensation methods were comparable for a 3×3 grid, we also performed the same test on our 11×27 taxel sensor that we attached to the soft robot in earlier tests. We only tested using the resistance model method

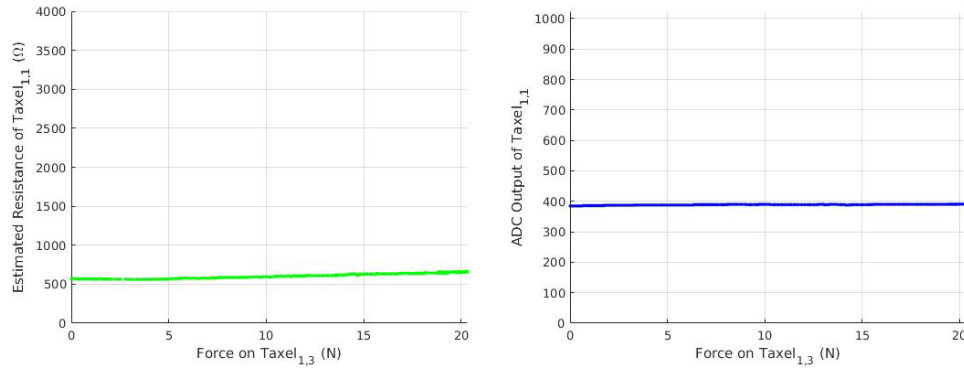


Figure 17. Left: validation of cross-talk compensation for the method of modeling the circuit. Right: validation of cross-talk compensation using the diode/multiplexer method.

Table 1. Comparison of percent changes for the uncompensated graph and the two compensation methods.

Force range	Percent change for compensation methods		
	Uncompensated	Resistance model	Extra circuitry
0–20 N	1.0114	0.1182	0.0234
0–5 N	1.3726	0.0346	0.0745

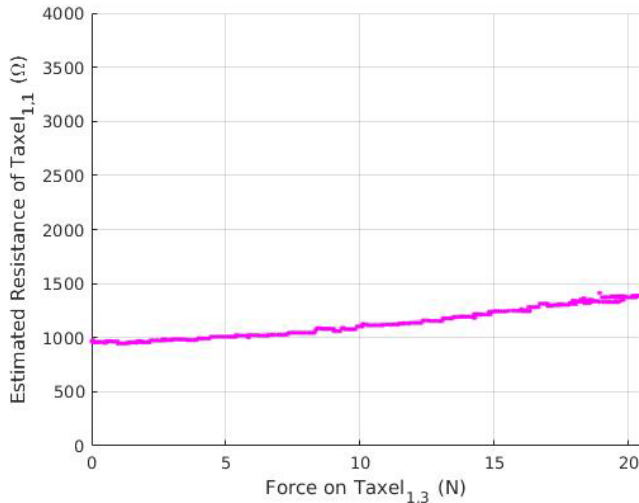


Figure 18. The effects of cross-talk on an 11×27 taxel sensor.

(see section 4.1), and the results are shown in figure 18. The cross-talk compensation is still most effective below 5 N when scaled, but as the force increases the cross-talk compensation begins to degrade. Interestingly, this only seemed to be true for the resistance model version, and also occurred in the 3×3 version (table 1). We expect that this is caused by the ADC resolution and the fact that the sensor is only powered by 5 V. Since the voltage range for each taxel decreases as the number of taxels increases, an ADC with higher resolution is needed to capture smaller changes in voltage that are necessary for calculating the resistance accurately. Despite this limitation in our current hardware implementation, when the sensor is in use on soft robots, the total force will be distributed among multiple taxels where each taxel will experience a relatively small force as shown in section 4.1.4. This means that the high resolution sensor in its current configuration can still estimate forces accurately for a certain range of forces per taxel.

5. Conclusion

This paper has presented robust tactile sensor arrays that can measure contact over large areas, which is something that is difficult for most other current designs. Additionally, the sensor design is flexible and scalable for manufacturing, which makes it an ideal candidate for integration for future applications with soft robots. We have presented two methods for overcoming cross-talk. The effects of parallel parasitic cross-talk can be modeled and used to calculate the actual resistance at each taxel and correlated to force, or cross-talk can be eliminated through additional circuitry, i.e. multiplexers and diodes, so that voltage output can be directly correlated to force. The first method allows sensors to be built with minimal circuitry at low cost, and the second method simplifies the typical switching method in the literature by using diodes to stop the negative flow of current through the circuit. Both methods are effective at showing contact locations and estimating forces applied to the tactile sensor. We expect that these results, coupled with past research on whole-body tactile sensing for control in cluttered environments (see [28, 29]), should enable soft robots to more effectively interact with the real world. Additionally, the low cost of having such a large number of sensors enabled by our methods may be useful for learning data-driven models of soft robots and soft robot interaction, given the inherent difficulty in modeling them analytically.

Acknowledgments

This work was supported in part by an Early Career Faculty grant from NASA's Space Technology Research Grants Program (to MDK), a NASA SBIR Phase II grant (to MDK), the National Science Foundation Award 1461547 (to VJS), and the Office of Naval Research Award N00014-16-1-2468 (to VJS). We wish to acknowledge Kevin Albert and his team

at Pneubotics (an affiliate of Otherlab Company) for collaboration in regards to the soft robot hardware platform. We also thank Eric Peltola for assistance with circuit diagram edits and Eunsuk Chong for assistance with videography.

Appendix. Index to supplementary multimedia attachments

Number	Type	Description
1	Video	Reduction of cross-talk for tactile sensor array as described in section 4.1.3
2	Video	Experiment described in section 4.1.4 comparing tactile sensor data on a soft robot to ground truth data
3	Video	Demonstration of second method of cross-talk reduction described in section 4.2.1
4	Video	Example application of second method of cross-talk reduction on a soft-bodied human wrist described in section 4.2.2

ORCID iDs

Veronica J Santos  <https://orcid.org/0000-0003-3684-0733>

Marc D Killpack  <https://orcid.org/0000-0001-9372-104X>

References

- [1] Sanan S, Moidel J B and Atkeson C G 2009 Robots with inflatable links *IEEE/RSJ Int. Conf. on Intelligent Robots and Systems* (IEEE) pp 4331–6
- [2] Best C M, Gillespie M T, Hyatt P, Rupert L, Sherrod V and Killpack M D 2016 A new soft robot control method: using model predictive control for a pneumatically actuated humanoid *IEEE Robot. Autom. Mag.* **23** 75–84
- [3] Wilson J P, Best C M and Killpack M D 2017 Variable stiffness adaptation to mitigate system failure in inflatable robots *IEEE Int. Conf. on Robotics and Automation* (IEEE) pp 5844–51
- [4] Ilev O 2009 Soft fluidic actuators of rotary type for safe physical human-machine interaction *IEEE Int. Conf. on Rehabilitation Robotics* (IEEE) pp 1–5
- [5] Yuen M C, Tonoyan H, White E L, Telleria M and Kramer R K 2017 Fabric sensory sleeves for soft robot state estimation *IEEE Int. Conf. on Robotics and Automation* (IEEE) pp 5511–8
- [6] Mosadegh B, Polygerinos P, Keplinger C, Wennstedt S, Shepherd R F, Gupta U, Shim J, Bertoldi K, Walsh C J and Whitesides G M 2014 Pneumatic networks for soft robotics that actuate rapidly *Adv. Funct. Mater.* **24** 2163–70
- [7] Felt W, Chin K Y and Remy C D 2016 Contraction sensing with smart braid mckibben muscles *IEEE/ASME Trans. Mechatronics* **21** 1201–9
- [8] Marchese A D, Tedrake R and Rus D 2016 Dynamics and trajectory optimization for a soft spatial fluidic elastomer manipulator *Int. J. Robot. Res.* **35** 1000–19
- [9] Rus D and Tolley M T 2015 Design, fabrication and control of soft robots *Nature* **521** 467
- [10] Bhattacharjee T, Jain A, Vaish S, Killpack M D and Kemp C C 2013 Tactile sensing over articulated joints with stretchable sensors *2013 World Haptics Conf.* (IEEE) pp 103–8
- [11] Canavese G, Stassi S, Fallauto C, Corbellini S, Cauda V, Camarchia V, Pirola M and Pirri C F 2014 Piezoresistive flexible composite for robotic tactile applications *Sensors Actuators A* **208** 1–9
- [12] Kerpa O, Weiss K and Worn H 2003 Development of a flexible tactile sensor system for a humanoid robot *Proc. 2003 IEEE/RSJ Int. Conf. on Intelligent Robots and Systems* vol 1 (IEEE) pp 1–6 (Cat. No.03CH37453)
- [13] Russell R 1987 Compliant-skin tactile sensor *IEEE Int. Conf. on Robotics and Automation. Proc.* vol 4 (IEEE) pp 1645–8
- [14] Shimojo M, Namiki A, Ishikawa M, Makino R and Mabuchi K 2004 A tactile sensor sheet using pressure conductive rubber with electrical-wires stitched method *IEEE Sens. J.* **4** 589–96
- [15] Strohmayr M, Saal H P, Potdar A and Van Der Smagt P 2010 The DLR touch sensor I: a flexible tactile sensor for robotic hands based on a crossed-wire approach *IEEE/RSJ Int. Conf. on Intelligent Robots and Systems* (IEEE) pp 897–903
- [16] Rogers J A, Someya T and Huang Y 2010 Materials and mechanics for stretchable electronics *Science* **327** 1603–7
- [17] Lu N, Lu C, Yang S and Rogers J 2012 Highly sensitive skin-mountable strain gauges based entirely on elastomers *Adv. Funct. Mater.* **22** 4044–50
- [18] Someya T, Kato Y, Sekitani T, Iba S, Noguchi Y, Murase Y, Kawaguchi H and Sakurai T 2005 Conformable, flexible, large-area networks of pressure and thermal sensors with organic transistor active matrixes *Proc. Natl Acad. Sci. USA* **102** 12321–5
- [19] Someya T, Sekitani T, Iba S, Kato Y, Kawaguchi H and Sakurai T 2004 A large-area, flexible pressure sensor matrix with organic field-effect transistors for artificial skin applications *Proc. Natl Acad. Sci. USA* **101** 9966–70
- [20] Yamaguchi A and Atkeson C G 2016 Combining finger vision and optical tactile sensing: reducing and handling errors while cutting vegetables *IEEE-RAS 16th Int. Conf. on Humanoid Robots (Humanoids)* (IEEE) pp 1045–51
- [21] Sareh S, Jiang A, Faragasso A, Noh Y, Nanayakkara T, Dasgupta P, Seneviratne L D, Wurdemann H A and Althoefer K 2014 Bio-inspired tactile sensor sleeve for surgical soft manipulators *IEEE Int. Conf. on Robotics and Automation* (IEEE) pp 1454–9
- [22] Yang Y-J, Cheng M-Y, Shih S-C, Huang X-H, Tsao C-M, Chang F-Y and Fan K-C 2010 A 32 × 32 temperature and tactile sensing array using PI-copper films *Int. J. Adv. Manuf. Technol.* **46** 945–56
- [23] Yang Y-J, Cheng M-Y, Chang W-Y, Tsao L-C, Yang S-A, Shih W-P, Chang F-Y, Chang S-H and Fan K-C 2008 An integrated flexible temperature and tactile sensing array using pi-copper films *Sensors Actuators A* **143** 143–53
- [24] Wu J and Wang L 2016 Cable crosstalk suppression in resistive sensor array with 2-wire S-NSDE-EP method *J. Sens.* **2016** 1–9
- [25] Zhang T, Liu H, Jiang L, Fan S and Yang J 2013 Development of a flexible 3D tactile sensor system for anthropomorphic artificial hand *IEEE Sens. J.* **13** 510–8
- [26] Horii T, Nagai Y, Natale L, Giovannini F, Metta G and Asada M 2014 Compensation for tactile hysteresis using gaussian process with sensory markov property *2014 14th IEEE-RAS Int. Conf. on Humanoid Robots (Humanoids)* (IEEE) pp 993–8
- [27] 1998 *High-Speed CMOS Logic 16-Channel Analog Multiplexer/Demultiplexer CD74HC4067*, Revised July 2003, Texas Instruments
- [28] Jain A, Killpack M D, Edsinger A and Kemp C C 2013 Reaching in clutter with whole-arm tactile sensing *Int. J. Robot. Res.* **32** 458–82
- [29] Killpack M D, Kapusta A and Kemp C C 2016 Model predictive control for fast reaching in clutter *Auton. Robots* **40** 537–60